Demonstration of Multipulsed Current Drive Scenario using Coaxial Helicity Injection in the HIST Spherical Torus Plasmas

M. Nagata 1), T. Higashi 1), T. Kanki 2), K. Ando 1), Y. Kikuchi 1), N. Fukumoto 1),
Y. Kagei 3)

1) Univerisity of Hyogo, Himeji, Hyogo, Japan
2) Japan Coast Guard Academy, Kure, Hiroshima, Japan
3) Research Organization for Information Science & Technology, Tokai, Ibaraki, Japan

E-mail contact of main author: nagata@eng.u-hyogo.ac.jp

Abstract. The Helicity Injected Spherical Torus (HIST) device has been developed towards high-current start up and sustainment by Mutipulsed Coaxial Helicity Injection (M-CHI) method. Multiple pulses operation of the coaxial plasma gun can build the magnetic field of spherical torus (ST) and spheromak plasmas in a stepwise manner. Successive double gun pulses have been demonstrated to amplify the magnetic field and the plasma current against resistive decay. The resistive 3D-MHD numerical simulation has reproduced the current amplification by the M-CHI method and confirmed that stochastic magnetic field is reduced so that closed flux surfaces are repeatedly created during the resistive decay process. These experimental and computational results from STs have provided, for the first time, availability of a quasi-steady-state "refluxing" mode in which the magnetic field is allowed to decay partially before being rebuilt. Our goal is to achieve simultaneously the good energy confinement and the current sustainment by the M-CHI method.

1. Introduction

Non-inductive plasma startup and current drive by CHI using a magnetized coaxial plasma gun (MCPG) have been successfully demonstrated for spheromak (CTX, SPHEX, FACT, SSPX) and ST plasmas (HIT-II, HIST, NSTX) that have a potential to lead to an attractive steady-state high-beta fusion reactor [1-4]. An anticipated issue for CHI is achieving good energy confinement, since it relies on the magnetic relaxation that involves a n=1 kink instability on the open flux column produced around the central post. Recent SSPX results indicate that high temperatures cannot be sustained in steady state by CHI [1]. This is essentially because CHI cannot drive a dynamo directly inside a closed magnetic flux surface, so that the field lines become stochastic and therefore the flux surface is only an approximate, i.e. "mean-field" one during the sustainment. In order to improve this weak point of the CHI, the pulsed operation scenario of CHI, i.e. "Multipulsed drive", "Refluxing" mode, or "Repetitive plasmoid injection and merging" mode has been proposed to achieve quasi-steady-state sustainment with partial recovery of plasma current between field-building pulses [5]. A second pulse injection of helicity would stop the ramp-down and rebuild the plasma current after it has decreased resistively. This process then repeats, yielding a quasi-steady-state plasma with low energy loss. This multipulse operation has been for the first time demonstrated in the SSPX gun-spheromak device [5,6] and also for RFP reactor designs [7], the similar operation scenario using Oscillating Field Current Drive (OFCD) has already been proposed. We wish to achieve good energy confinement and sustainment simultaneously by the multipulse operation.

The main purpose of this experiment is to examine the multipulsed operation scenario in the low-q and high-q ST configurations. We will investigate mechanism to recreate successfully the magnetic fields and effect of flow on current amplification. To begin with M-CHI experiments, we have started the initial experiment from a double pulsed operation. In this paper, we have presented the time evolution of the internal magnetic field structures, the

redistribution of the toroidal current density occurred by transition to the decay phase from the driven phase, MHD dynamo and comparison to computational results from the 3D-MHD simulation.

2. The HIST devise and diagnostics

A schematic view of the HIST device ($R = 0.30$ m, $a = 0.24$ m, $A = 1.25$) and diagnostics used in this experiment is shown in Fig. 1. The structures, sizes, capabilities, diagnostics, and operating conditions of HIST are described in detail in Ref. [2], but some diagnostic and additional capacitor bank systems for M-CHI are also described briefly here. The capacitor banks ($V_{max} = 10$ kV, $C = 0.6$-2.6 mF) are used for ST formation. The two sustainment banks ($V_{max} = 900$ V, $C = 195$ mF and 335 mF) have been prepared for the double gun pulse operation in this experiment.

The HIST device has surface poloidal pick-up coils, λ-probe, internal magnetic probing arrays, a toroidal mode probe, Ion Doppler Spectrometer (IDS), Dynamo-Mach probes and a CO_2 laser interferometer. Three axis magnetic probes (B_r, B_θ, B_z) are inserted in the plasma at a distance of $z = 0.074$ m from the midplane ($z = 0$ m) of the spherical solid copper flux conserver (FC) (diameter: 1.0 m, thickness: 3 mm). Magnetic pick-up coils (16 channels for B_z) are located in the poloidal direction along the inner surface of the FC to calculate the total toroidal plasma current I_t. A six channels λ-probe incorporating small size Rogowski and flux loops is used to measure toroidal current density J_t and local toroidal flux Ψ_t profiles on the FC midplane. The toroidal n-mode number of the magnetic fluctuations of B_t is measured using eight magnetic pick-up coils distributed toroidally at equal angles over 360 degrees and around $R = 0.15$ m. The line averaged electron density are measured by a CO_2 laser interferometer with a single tangential chord ($R = 0.24$ m) on the midplane. The IDS system using a compact 16 channel photomultiplier tube, optical fibers and 1 m-spectrometer (resolution: 0.0085nm) has been developed in order to measure ion temperature $T_{i.D}$ and ion flow velocity $v_{i.D}$. Technical details of the similar IDS system are reported in Ref. [8]. In this experiment, the optical fiber covered with glass tubes is inserted into the plasma, and so the radial profile of $T_{i.D}$ and $v_{i.D}$ can be measured. MHD dynamo electric field and ion flow measurements have been conducted by three axis Dynamo-Mach probes. The Dynamo-Mach probe consists of nine tungsten rods surrounding glass-ceramic (Macor) and three axis magnetic pick-up coils. Ion flows and magnetic fields can be simultaneously measured in the three axis directions. An ion flow velocity v_i is calculated by $v_i = C_s M_i$, where C_s is an ion sound velocity (~30 km/s, $T_e = T_i$). An ion Mach number M_i can be obtained from $M_i = M_c \ln(J_{up}/J_{down})$, where M_c is a proportionality constant that depends on T_e and T_i, and where J_{up} and J_{down} are ion current densities measured by upstream and downstream rod probes, respectively. Because the probe radius is smaller than the ion Larmor radius (>1 cm), the
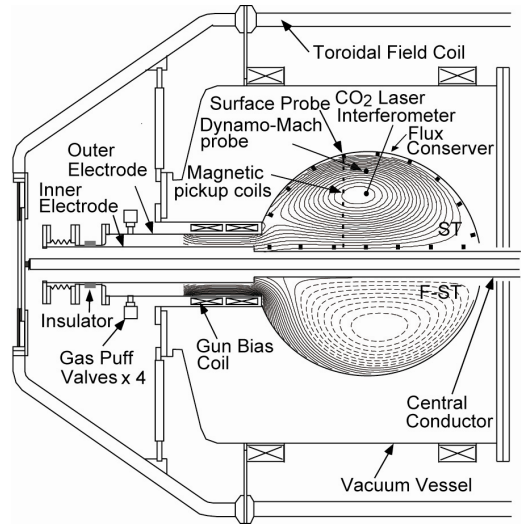

FIG.1 Schematic diagram of the HIST device and diagnostics.

unmagnetized condition is satisfied in the theoretical model which determines $M_c = 0.53$ (assuming that $T_e = T_i$) in this case.

3. Experimental results

3.1. Typical CHI discharges with driven and decay phases

The HIST device can form and sustain the ST (high-q: $q > 1$ and low-q including spheromaks: $q < 1$) by utilizing the variation of the external toroidal field (TF) coil current I_{tf}. By operating the MCPG with $\lambda_{gun} > \lambda_{FC}$, here $\lambda_{gun} = \mu_0 I_{gun}. / \Psi_{bias}$ and λ_{FC} is the flux conserver eigenvalue ($\lambda_{FC} = 8.53$), required for a helicity-driven ST, we can inject helicity continuously into the plasma. Figure 2 shows a comparison between the high-q and low-q ST plasmas. The injection gun current is $I_{gun} \sim 30$ kA in both operations and the gun bias flux Ψ_{bias} is adjusted properly. The toroidal plasma current I_t in each condition has been amplified up to 110 kA and 80 kA, respectively. The flux amplification (FA) rate ($= \Psi_p / \Psi_{bias}$) of the low-q ST is higher than that of the high-q ST. During the driven phase ($t < 1.7$ ms), magnetic fluctuations have been observed in both conditions. The amplitude of the fluctuation (< 30 kHz) in the low-q is larger than in the high-q. The toroidal component ($<\tilde{v}_z \tilde{B}_r - \tilde{v}_r \tilde{B}_z>$) of the dynamo

electric field $<\tilde{v} \times \tilde{B}>$ in the low-q case is peaked around 20 V/m. The strong dynamo action causes the high FA during the driven phase. After the gun current drops below the threshold for driving the fluctuation, the resistive decay becomes dominant, leading to the reduction of the observed dynamo fluctuations.

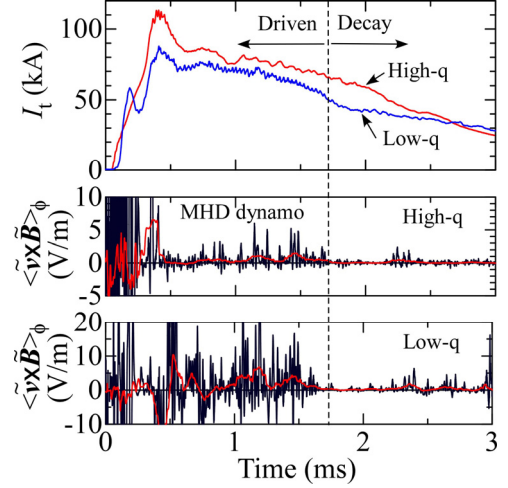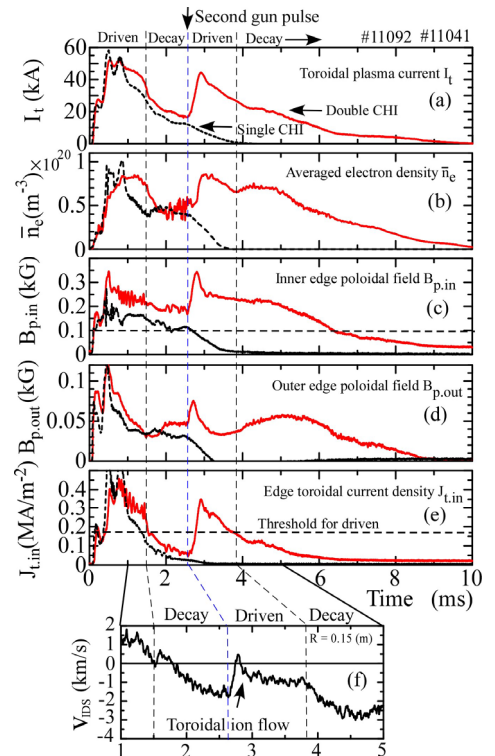*FIG. 2. Time evolution of the toroidal plasma current of high-q (#10852, $I_{tf} = 158$ kAturns) and low-q ST (#10857, $I_{tf} = 39$ kAturns) plasmas and the dynamo electric field signal (R=0.35 m, Z=0 m) in each discharge.*

3.2. Double pulses operation results

The low-q ST plasma with $I_t \sim 60$ kA is initially produced by the formation bank and the first sustainment bank. Thereafter, the other sustainment bank is fired at $t \sim 2.5$ ms to apply the second gun pulse between electrodes. Figure 3 illustrates temporal evolutions of I_t, $<n_e>$, $B_{p.in}$, $B_{p.out}$ and $J_{t.in}$.

FIG. 3. Time evolution of (a) I_t, (b) $<n_e>$, (c) $B_{p.in}$ (R=0.15 m), (d) $B_{p.out}$ (R=0.45 m), (e) $J_{t.in}$ (R=0.1 m) in the comparison of single and double pulsed discharges, and (f) toroidal flow velocity measured by IDS in the double pulse discharge.

By pulsing the MCPG at $t \sim 2.5$ ms during the decaying of the initial plasma, we have observed that I_t is effectively amplified against the resistive decay. In addition, the life time t_{life} has increased up to ~10 ms which is longer than that in the single CHI case ($t_{life} \sim 4$ ms). The edge fields, $B_{p.in}$ and $B_{p.out}$ last between $t = 0.5$ ms and $t = 6$ ms like a repetitive manner as shown by Fig.3 (c) (d). After $t \sim 6$ ms, the poloidal fields decay exponentially. Fig.3 (e) shows that the $J_{t.in}$ produced mainly by the injected gun current drops down quickly which means the peaking of the current profile during the decay phase. After the $J_{t.in}$ drops below a threshold for driving the $n=1$ mode, magnetic fluctuations (~20 kHz) seen on the signal of $B_{p.in}$ are reduced during the decaying phase (1.5 ms $< t <$ 2.6 ms). The fluctuation after the second pulse cannot be seen clearly in this shot. During the second driven phase (0.26 ms $< t <$ 3.8 ms), the toroidal flow ($v_{IDS} \sim 2$ km/s) measured by the IDS has been generated in background flow as shown by Fig.3 (f). The flow is driven in the same direction as I_t as well as in the formation and the first driven phase (0 ms $< t <$ 1.5 ms). Consequently, we may conclude that the successful merging process with the plasmoid injected additionally from the MCPG leads to the current amplification and the flow generation.

3.3. Internal magnetic field and current profiles

Figure 4 (a) shows the time evolution of internal poloidal magnetic field B_p profile in the double pulses discharge. The poloidal field strength is enhanced locally in the central open column (0.05 m$< R <$0.15 m) during the driven phase so that the magnetic axis appears to move nearer the inboard side. The toroidal field inside the central open column is slightly decreased from the vacuum field, i.e. "diamagnetic" due to a high pressure. In the decay phase, the magnetic axis tends to move towards the position of $R \sim 0.24$ m where is predicted by equilibrium calculations. The second pulse increases the B_p and the magnetic axis moves back near $R \sim 0.2$ m since the injected current flows along the central open field lines. After the short driven time (2.5 ms $< t <$ 3.8 ms), the plasma starts to experience again the decay process and the magnetic axis appears to remain around $R \sim 0.24$ m. The toroidal current density J_t shows a hollow profile in the driven phase as shown by Fig. 4 (b) and during the decay phase the driven-current diffuses towards the core region, leading to a peaked profile.
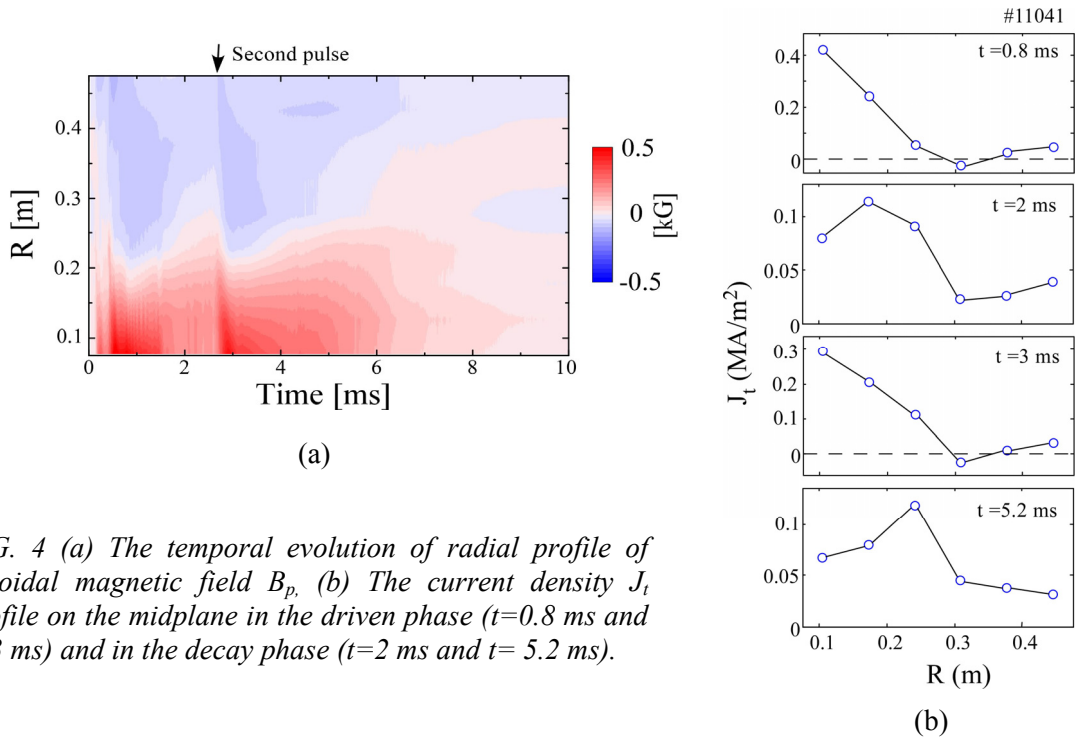

(a)

FIG. 4 (a) The temporal evolution of radial profile of poloidal magnetic field B_p, (b) The current density J_t profile on the midplane in the driven phase (t=0.8 ms and t=3 ms) and in the decay phase (t=2 ms and t= 5.2 ms).

(b)

The current inward diffusion results in the formation of equilibrium configurations. This transition process from a follow current profile to a peaked one is repeated in the same manner in the multipulse operation.

4. 3D-MHD numerical simulation results

The M-CHI for the sustainment of the low-q ST has been investigated using resistive, single-fluid 3D-MHD numerical simulations (MHDTM-code) [9,10]. All variables are treated in a normalized form. The length, magnetic field, and number density are normalized by the maximum length of the cylinder radius, $L_0 = 0.5$ m, the strength of the characteristic magnetic field, $B_0 = 0.2$ T, and the initial ion number density in the hydrogen plasma, $n_0 = 5.0 \times 10^{19}$ m^{-3}, respectively. Under these normalizations, the velocity, time and current are normalized by the Alfvén velocity, $v_A = 620$ km/s, the Alfvén transit time, $\tau_A = 0.81$ μsec, and the toroidal plasma current $I_t = 80$ kA, respectively. We adopt the simulation system shown in Fig. 5 and use a 3D full-toroidal cylindrical (r, θ, z) geometry. The simulation region is divided into two cylinders with a central conductor inserted along the symmetry axis. One is a gun region ($0.175 \le r \le 0.65$ and $0 \le z \le 0.5$), and the other is a confinement region ($0.15 \le r \le 1.0$ and $0.5 \le z \le 2.0$). The insertion of a toroidal field current I_{tf} along the geometry axis inside the central conductor produces a vacuum toroidal field, creating the low-q ST configuration by setting $I_{tf} = 0.4$. A bias magnetic flux penetrates electrodes at the inner and outer boundaries of the gun region to drive the plasma current by applying an electric field. We use a perfect conducting boundary at the wall of the confinement region. The initial conditions for the simulation are given by an axisymmetric MHD equilibrium, which can be obtained by numerically solving a Grad-Shafranov equation derived from a force-free relation $\nabla \times \boldsymbol{B} = \lambda \boldsymbol{B}$, under these boundary conditions. Here λ is the force-free parameter, defined by $\lambda \equiv \boldsymbol{j} \cdot \boldsymbol{B}/B$, representing the current density parallel to the magnetic field. The parameters used in the simulation are force-free parameters at the magnetic axis,
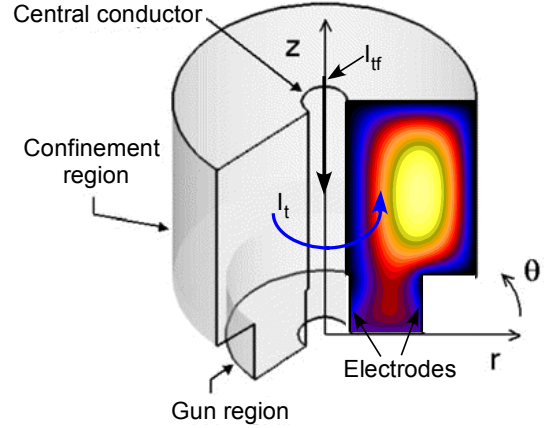

FIG. 5. Schematic view of simulation geometry in cylindrical coordinates (r, θ, z). Blue arrow indicates the direction of toroidal current I_t
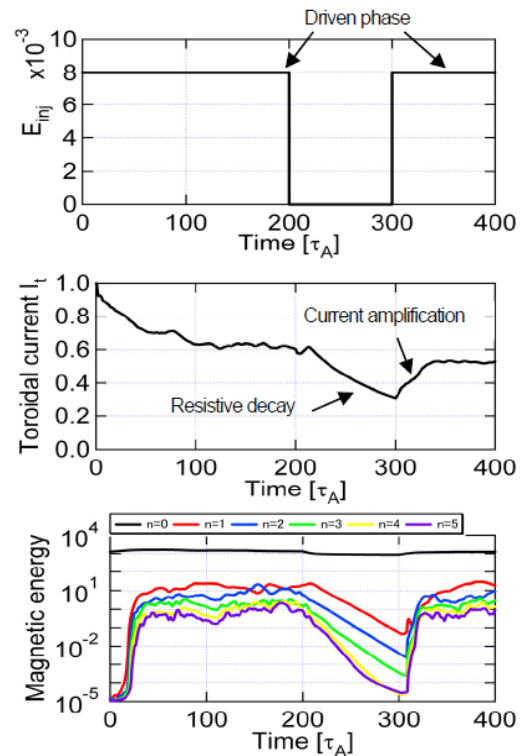

FIG. 6. Time evolution of the toroidal current I_t and magnetic energy W_{mag} for the toroidal Fourier mode when a toroidally symmetric radial electric field E_{inj} is applied in the shape of pulses.

λ_{axis} = -3.5, and at the separatrix, λ_{s} = -3.3, and the safety factors at the magnetic axis, q_{axis} = 1.3 and at the separatrix, q_{s} = 2.4, corresponding to a partially relaxed low-q ST configuration. The poloidal flux contours with the axisymmetric MHD equilibrium used as the initial condition are shown in Fig. 5. In addition, the conductivity κ, viscosity μ, and resistivity η are assumed to be 1.0×10^{-3}, 1.0×10^{-3}, and 2.0×10^{-4}, respectively. During the driven phase ($0\,\tau_{\text{A}} < t < 200\,\tau_{\text{A}}$ and $300\,\tau_{\text{A}} < t < 400\,\tau_{\text{A}}$), a toroidally symmetric radial electric field E_{inj} of 8.0×10^{-3} is applied to the gap between gun electrodes, while during the decaying phase ($200\,\tau_{\text{A}} < t < 300\,\tau_{\text{A}}$), it is not applied. In the simulation, the mass density is spatially and temporally constant, and no-slip wall condition is assumed at all boundaries of the simulation region.

On the basis of the simulation results, the effects of the M-CHI on dynamics of the low-q ST have been investigated. Figure 6 shows the time evolution of the toroidal current I_{t} and magnetic energy W_{mag} for the toroidal Fourier mode. As shown in Fig. 6, I_{t} is successfully sustained against resistive dissipation during the driven phase. After E_{inj} vanishes at $t = 200\,\tau_{\text{A}}$, I_{t} starts to decay due to the resistivity. When E_{inj} is applied again at $t = 300\,\tau_{\text{A}}$, I_{t} increases from 0.31 to 0.53 for 40 τ_{A}, resulting in the effective current amplification. This result agrees
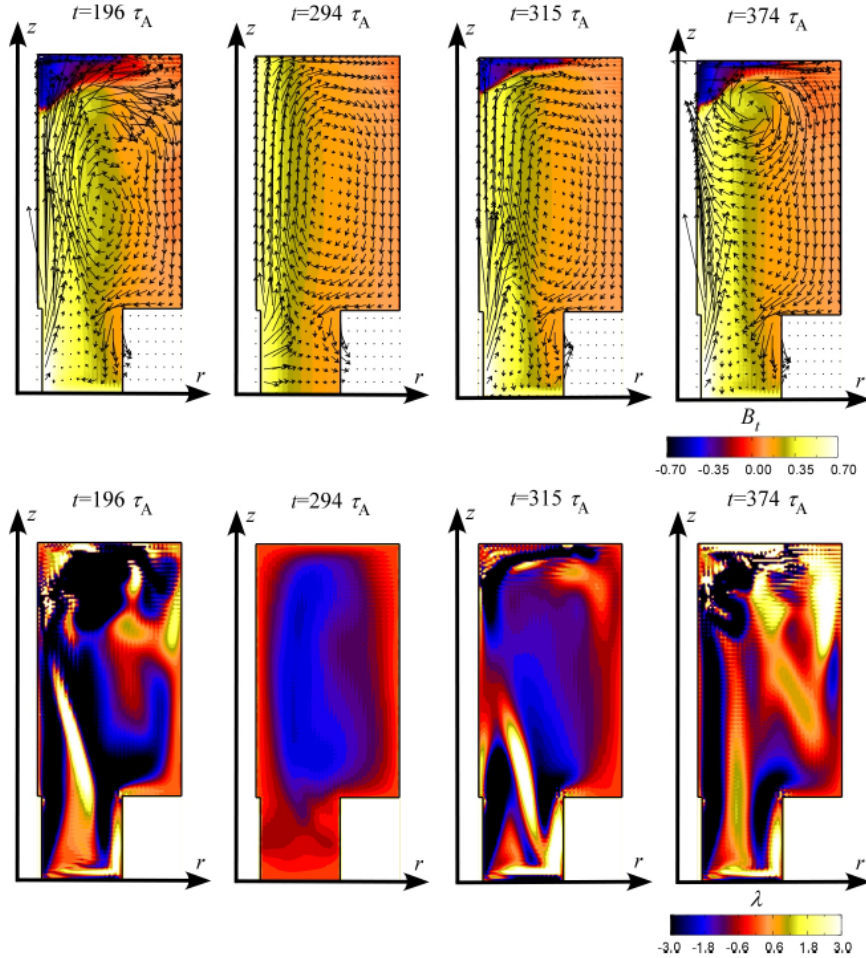

FIG.7. Time evolution of magnetic fields and λ profiles on the poloidal cross section at the $\theta = 3\pi/2$ plane. Upper panels indicate the vector plots of poloidal field and the contours of toroidal field, and lower ones indicate the λ profiles. Color of the toroidal field varies from black to blue, red, yellow, and white as the toroidal field increases. Color of the λ varies from black to blue, red, yellow, and white as the λ increases.

with the observations on HIST. The magnetic fluctuation energy is relatively large magnitude during the driven phase. After E_{inj} is not applied at $t = 200\,\tau_A$, the $n = 1\text{-}5$ components decay until application of E_{inj} at $t = 300\,\tau_A$, indicating to relax to an axisymmetric state. When E_{inj} is applied again at $t = 300\,\tau_A$, the $n =$ 1-5 components grow up to the original levels. Figure 7 shows the time evolution of magnetic fields and λ profiles on the poloidal cross section. The sustained low-q ST during the driven phase has helical distortion of the open magnetic field lines around the central conductor, i.e., the central open column. When the gun current along the central open column is increased by E_{inj}, a critical current density gradient is attained, and the central open column violates the Kruskal-Shafranov kink stability criterion. The $n = 1$ kink mode is destabilized, leading to the experimentally observed helical distortion. At $t = 196\,\tau_A$, and $t = 374\,\tau_A$, the $n = 1$ kink instability causes the helical distortion by overcoming a stabilized effect due to the vacuum toroidal field produced by I_{tf}. The nonlinear evolution of the helical kink distortion is considered to produce a dynamo electric field, leading a current drive. At these times, λ is always provided from the gun to the confinement region and is concentrated on a periphery region, particularly the central open column. Also, λ has the same direction as I_t (blue) except for the current sheets (yellow). The current sheets around the gun muzzle and the upper part of the confinement region are generated by the twisting of magnetic field lines. During the decaying phase ($E_{inj}= 0$), the magnetic fluctuation energy dissipates and the amount of closed field lines increases. At $t = 294\,\tau_A$, the helical distortion of the central open column vanishes and then ordered magnetic field structures are formed. Also, λ concentrated on the central open column diffuses toward the core region so as to reduce the gradient in λ or J_t, relaxing in the direction of the Taylor state. These results agree well to the experimental results. Therefore, it is expected that by effectively controlling M-CHI, the magnetic fluctuations induced during the driven phase are suppressed and the current density in the central open column is redistributed to the core region during the decaying phase, resulting in the current amplification and improving confinement.

5. Summary

We have confirmed experimentally and computationally the availability of the M-CHI method to hold magnetic fields at quasi-steady-state value though each successive pulse. It has been observed that the current concentrated in the central open column during the driven phase diffuses towards the core region and as a result, the peaked current profile is formed in the decay phase. The periodic driven and decay processes could be provided by the dynamo current drive and the generation of closed flux surfaces during the flattening of λ profile. In order to approach the key goal of this research, we need to investigate MHD dynamo and to control the n=1 kink instability of the open central column.

References
[1] McLEAN, H. S., *et al.*, Phys. Rev. Lett. **88** (2002) 125004.
[2] NAGATA, M, *et al.*, Phys. Plasmas **10** (2003) 2932.
[3] REDD, A. J., *et al.*, Phys. Plasmas **14** (2007) 112511.
[4] RAMAN, R., *et al.*, Phys. Rev. Lett. **97** (2006) 175002.
[5] WOODRUFF., *et al.*, Phys. Rev. Lett. **90** (2003) 095001.
[6] HUDSON, B., *et al.*, Phys. Plasmas **15** (2008) 056112.
[7] NEBEL, R.A., *et al*., Phys. Plasmas **9** (2002) 4968.
[8] GU. P., *et al*., Rev. of Sci. Instrum. **75** (2004) 1337.
[9] KAGEI, Y., *et al.*, J. Plasma Fusion Res. **79** (2003) 217.
[10] KANKI, T., *et al.*, J. Plasma Fusion Res. SERIES **8** (2009) 1167.